Force measurement in a nanomachining instrument

doi: 10.1063/1.1319976

Force measurement in a nanomachining instrument

Wei Gao[a)]
Department of Mechatronics and Precision Engineering, Tohoku University, Aramaki Aza Aoba 01, Sendai 980-8579, Japan

Robert J. Hocken,[b)] John A. Patten, and John Lovingood
Center for Precision Metrology, The University of North Carolina at Charlotte, 9201 University City Boulevard, Charlotte, North Carolina 28223

(Received 6 June 2000; accepted for publication 28 August 2000)

Two miniature, high sensitivity force transducers were employed to measure the thrust force along the in-feed direction and the cutting force along the cross-feed direction in a nanomachining instrument. The instrument was developed for conducting fundamental experiments of nanocutting especially on brittle materials. The force transducers of piezoelectric quartz type can measure machining forces ranging from 0.2 mN to 10 N. The submillinewton resolution makes it possible to measure the machining forces in the cutting experiments with depths of cut as small as the nanometer level. The stiffness and resonant frequency of the force transducers are 400 mN/nm and 300 kHz, respectively, which meet the specification of the instrument. A force transducer assembly is designed to provide a mechanism to adjust the preload on the force transducer and to decouple the measurement of forces. The assembly consists of three dual-axis circular flexures and a subframe. The axial stiffness of the flexures is designed to be greater than 6×10^7 N/m and the lateral stiffness of the flexures is designed to be 1×10^6 N/m to provide proper decoupling of forces. © *2000 American Institute of Physics.* [S0034-6748(00)01012-1]

I. INTRODUCTION

In mechanical machining, such as turning and grinding, cutting tools are used to remove material to generate desired shapes by applying machining forces on the workpiece.[1] The machining force is therefore a fundamental parameter to reflect the machining process, and force measurement has always been required for practical use and research purposes.[2,3]

On the other hand, diamond turning, which was developed in the 1960s, has created a new field of ultraprecision machining. Diamond turning is the use of a single-point diamond tool with a very sharp tool edge on a precision lathe under very precisely controlled machine and environmental conditions to fabricate precision parts.[4] In contrast to normal cutting practice, diamond turning can directly realize optical surface finish without subsequent lapping and polishing operations, which leads to the improvement of machining effectiveness and reduction of machining cost.[5] With the technique of fast tool servo, complicated forms can also be generated with high accuracy.[6,7] Currently submicrometer form accuracy and nanometer surface finish have been reached by commercially available diamond turning machines and a higher level of form accuracy and surface finish is required for satisfying the requirement of producing ultraprecision parts. Meanwhile, it is necessary to take finer cuts to reduce the possibility of subsurface damage, which is a significant need in the semiconductor and optical industries. One way to satisfy these requirements is to perform nanocutting by reducing the depth of cut to the nanometer level.[8] For this purpose, it is necessary to carry out fundamental nanocutting experiments and computer simulations to understand the machining mechanism of the nanocutting process.[9,10] Nanocutting experiments are also necessary for studying brittle-ductile transition regions in machining brittle materials.[11–13]

In nanometer cutting, the machining force is a more important factor than that in a traditional metal-cutting process. It has been verified that the machining force per unit depth of cut increases dramatically as the depth of cut is reduced to smaller than approximately 20 μm, which is called the ''size effect.''[14,15] The existence of the size effect indicates that the machining force is an important indicator of the nanometer cutting mechanism such as the currently unexplained complex material transition, and needs to be measured precisely.

A second generation of nanomachining instrument has been designed and built to perform fundamental experiments of nanocutting.[16,17] In this two-dimensional cutting instrument, two force transducers with high resolution, high stiffness, and high-frequency response were used to monitor the cutting and the thrust forces. In this article, the principle of force measurement and the design of the force transducer assembly are described. Some measurement results of machining forces are also presented.

II. PRINCIPLE OF FORCE MEASUREMENT

Figure 1 shows a model of two-dimensional cutting.[18,19] This model, in which the cutting edge is perpendicular to the direction of the cross-feed motion (the relative work-tool motion in the X direction), is known as the orthogonal cut-

[a)]Electronic mail: gaowei@cc.mech.tohoku.ac.jp
[b)]Electronic mail: hocken@uncc.edu

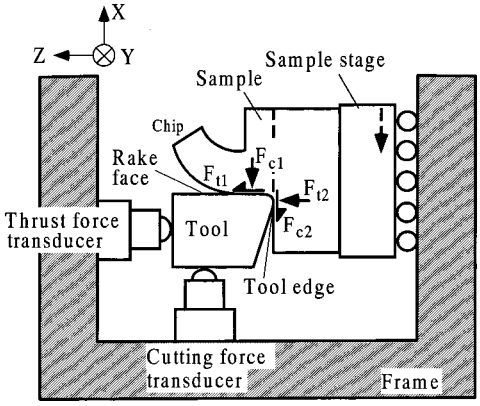

FIG. 1. Machining and force system model.

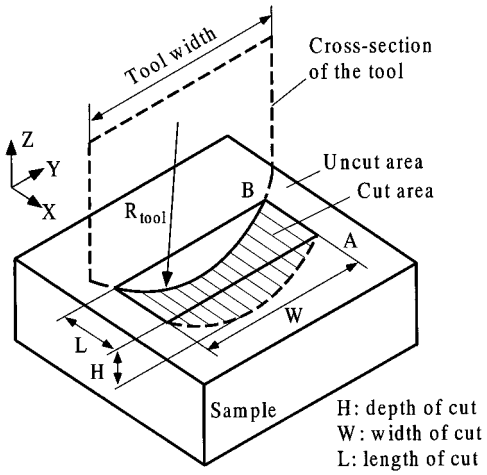

FIG. 2. Geometry of the orthogonal cutting using a round nose cutting tool.

ting model. Comparing with the practical three-dimensional cutting process, the orthogonal cutting model is much simpler and is suited to research investigations since many of the independent variables can be eliminated.[20]

A model of the force system is also shown in this figure.[21] The cutting force F_{cut} in the X direction and the thrust force F_{thrust} in the Z direction can be expressed as

$$F_{\text{cut}}=F_{c1}+F_{C2}=F_{c1}+\mu_1 F_{t2}, \tag{1}$$

$$F_{\text{thrust}}=F_{t1}+F_{t2}=\mu_2 F_{c1}+F_{t2}. \tag{2}$$

It can be seen that each directional force consists of two force components. F_{c1}, F_{t1} act at the rake face of the tool, and F_{c2}, F_{t2} act at the tool edge. μ_1 and μ_2 are the friction coefficients.

F_{cut} and F_{thrust} can be measured either by using a two-component force transducer or two single-component force transducers. There are also different types of force sensing. The strain gauge based force transducer, the displacement measurement based transducer and the piezoelectric crystal type transducer are examples. Since the force in nanocutting could be as small as several millinewtons, force transducers with submillinewton resolution are necessary. The stiffness and frequency response are also important factors. In addition, the force transducer should be compact and easy to assemble in the instrument. In the nanomachining instrument,[16] two single-component force transducers of piezoelectric type, which meet the requirements for the force measurement in nanocutting, are used. Table I shows the specifications of the force transducers.[22]

In the orthogonal cutting geometry, the geometry parameters are limited to the depth of cut, the width of cut, and the length of cut as shown in Fig. 2 where a round nose diamond tool is used. Assume that the maximum depth of cut is H, and the nose radius of the tool is R_{tool}. According to the geometric relationship shown in Fig. 2, the width of cut W can be expressed as

$$W=2\sqrt{2R_{\text{tool}}H-H^2}. \tag{3}$$

TABLE I. Specifics of the force transducer.

range	10 N
resolution	0.2 mN
sensitivity	2 mN/mV
resonant frequency	300 kHz
stiffness	400 mN/nm
linearity	1% F.S.
rise time	5 ms
discharge time constant	1 s
weight	8 g

III. FORCE TRANSDUCER ASSEMBLY

Figure 3 shows a photograph of the nanomachining instrument. The force transducers are mounted on the subframe of the force transducer assembly, which is described in detail in the next section. The whole instrument is assembled in a main frame constructed from stainless steel. A piezoelectric transducer (PZT) tube scanner is employed to accomplish a maximum depth of cut of 4 μm, and length of cut of more than 20 μm. The flexural stiffness and the axial stiffness of the PZT scanner are on the order of 10^6 and 10^7 N/m, respectively. The capacitance probe situated inside the PZT tube is used to monitor the Z-directional motion of the PZT. The measurement range of the capacitance probe is 2 μm.

A kinematic mount, which consists of three tungsten carbide balls resting in three silicon carbide V grooves, is designed to mount the sample holder. Figure 4 shows a photo-

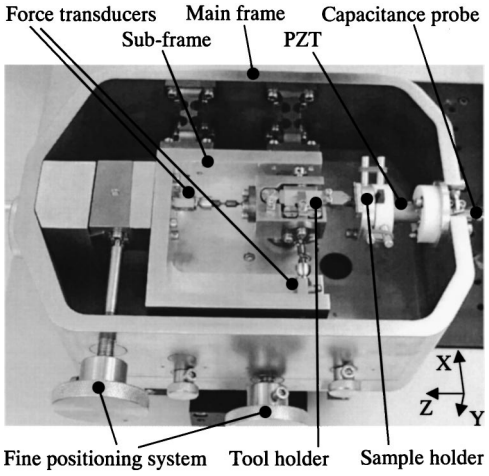

FIG. 3. Photograph of the nanomachining instrument.

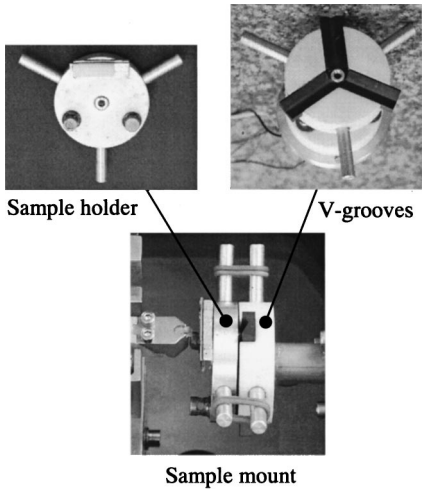

FIG. 4. Photograph of the kinematic sample mount.

graph of the kinematic mount. Two of the three balls are attached to screws, and the tilt of the sample in the $X-Y$ plane can be adjusted by rotating the two screws. The sample is glued at the top of the sample holder. Fine manual positioning systems are designed to provide smooth and repeatable motion for the force transducer assembly subframe. The subframe is supported by four dual-axis flexures, which attach to one side of the subframe. It is also actuated by a wedge in each axis.

The force transducer assembly houses the tool holder and the force transducers, which consists of the subframe, force transducers, and the tool holder assembly. The force transducers are mounted on the subframe, which is made of aluminum. Figure 5 shows a photograph of the tool holder assembly. The tool holder is supported at the bottom by a dual-axis flexure (flexure 1). Flexure 1 is used to provide motions of zero friction and backlash in the X and Z directions for the tool holder. As two single-component force transducers are used, it is necessary to decouple the measurement of the two forces. For this purpose, two more dual-axis flexures (flexures 2 and 3) are used. Flexures 2 and 3 are fixed to the side of the tool holder. The force transducers are preloaded against flexures 2 and 3 by using acorn nuts.

The stiffness and the natural frequency of the tool holder as well as those of the whole instrument are mainly determined by the three flexures used in the force transducer assembly. Figure 6 shows a schematic of the dual-axis flexures.

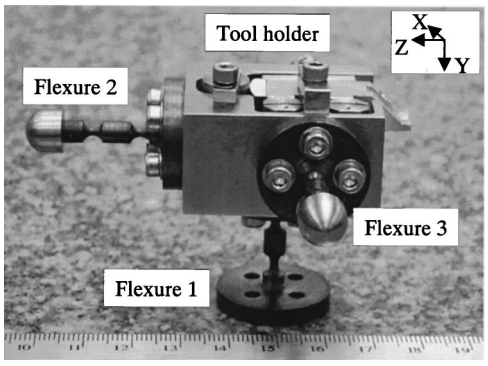

FIG. 5. Photograph of the tool holder assembly.

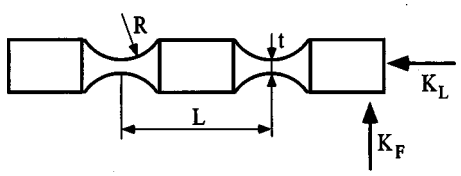

FIG. 6. Dual-axis flexure.

Flexures of the universal circular type are employed to accomplish the required rigidity along the longitudinal axis and compliance in the other two directions. The circular flexure is the simplest two-axis flexure with intersecting axes, which is formed by necking down a round bar.[23] Assume that the cutting radius of the hinge is R, the minimum hinge radius is t, and L is the length between the hinges. The stiffness along the longitudinal axis k_L (axial stiffness) and the stiffness along the cross axes k_F (flexural stiffness) can be expressed as[23]

$$k_L=\frac{Et^{3/2}}{4R^{1/2}}, \tag{4}$$

$$k_F=\frac{Et^{7/2}}{10L^2R^{1/2}}, \tag{5}$$

where E is the Young's modulus.

By choosing the following parameters: Hinge material: beryllium copper ($E=130$ GPa), $R=2.0$ mm, $t=2.0$ mm, and $L=10$ mm, k_L and k_F are designed to be

$$k_L=6.5\times10^7 \text{ N/m}, \tag{6}$$

$$k_F=1.0\times10^6 \text{ N/m}. \tag{7}$$

It can be seen that the axial stiffness k_L meets the requirement of being the same level as the axial stiffness of the piezoelectric tube scanner. The flexural stiffness k_F is two orders of magnitude smaller than the axial stiffness to realize the decoupling of measurement of the two forces. The force cross sensitivity is calculated to be 1.5% from k_F/k_L.

The natural frequency of the force transducer assembly can be calculated through

$$f=\frac{1}{2\pi}\sqrt{\frac{k_{F1}k_{L2}}{m(k_{F1}+k_{L2})}}=294 \text{ Hz}, \tag{8}$$

where k_{F1} is the flexural stiffness of flexure 1 for supporting the tool holder and k_{L2} is the axial stiffness of flexure 2 or

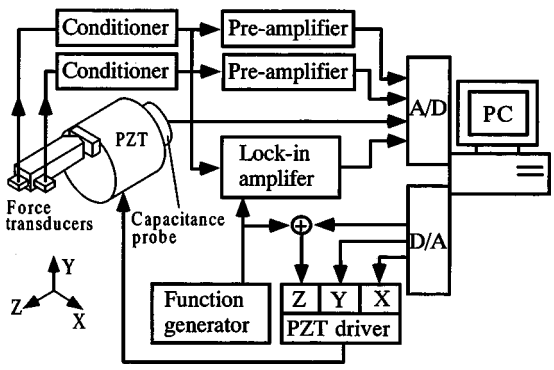

FIG. 7. Diagram of the experimental system.

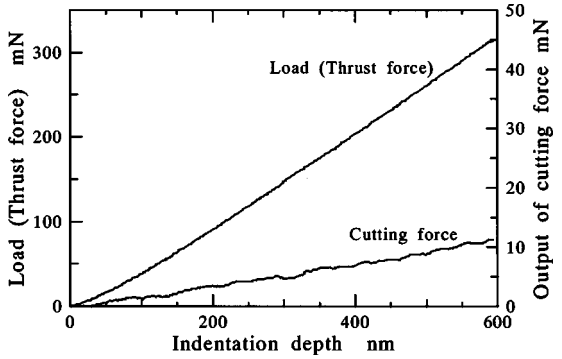

FIG. 8. Output of the thrust force transducer.

flexure 3 for force decoupling. *m* is the mass of the tool holder, which is approximately 0.3 kg in the instrument.

IV. EXPERIMENTS OF FORCE MEASUREMENT

Figure 7 shows a schematic of the system for nanomachining and force measurement experiments. The force transducers were first connected to PCB signal conditioners that are used to couple the force transducers. In the coupling process, the conditioner eliminates dc power bias from the output by means of a coupling capacitor. Since forces in nanomachining are considered to be very small, outputs of the signal conditioner are amplified by low-noise preamplifiers (Stanford Research Systems SR560). The gains of the preamplifiers are set to be between 20–100 in the experiments so that the force measuring sensitivity can reach higher values. A multichannel 16 bit analog/digital (A/D) board was used for data acquisition. Three 16 bit D/A converters are employed to control the three-dimensional motion of the piezoelectric tube scanner through a high-voltage PZT driver.

In nanomachining experiments, it is important to establish sample–tool contact to nanometer accuracy.[17] To make the tool–sample contact, the sample is automatically moved closer to the tool in the *Z* axis by using the PZT and small steps while monitoring the thrust force transducer output. To detect the small contact force, the sample is oscillated at an amplitude of 1 nm and a constant frequency (200 Hz) in the *Z* direction by the PZT, and the output of the force transducer is detected by a lock-in amplifier. An increase of the force transducer output at the oscillation frequency indicates

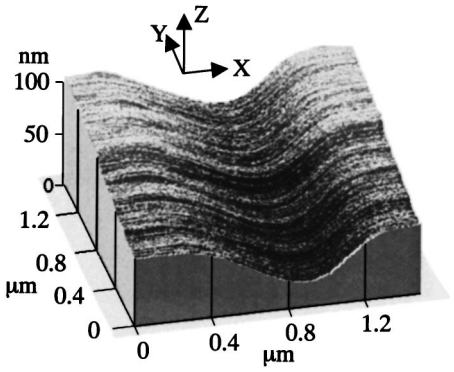

FIG. 9. AFM image of the indent.

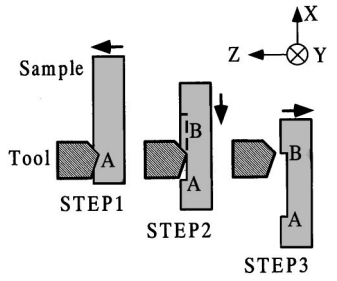

FIG. 10. Machining procedure.

the tool–sample contact, and the capacitance probe records the position of the PZT at the contact point. Once the tool–sample contact is established, the movement of the sample is automatically stopped and the oscillation amplitude of the sample is set to zero.

Indentation experiments were performed to evaluate the cross sensitivity of the two-dimensional force measurements. In an indentation experiment, only the *Z*-axis motion (in-feed motion) of the piezoelectric tube scanner is required to move the sample to the indenter. The indentation load was measured by the thrust force transducer and the indentation depth was measured by the capacitance probe. Figure 8 shows the output of the thrust force transducer with respect to the indentation depth. A diamond cutting tool was employed as the indentor. The round nose tool had a rake angle of $-45°$ and a clearance angle of 5°. The nose radius of the tool was 10 mm. During the loading procedure, the indentation displacement was incremented with a constant speed until the indentation displacement reached the programmed maximum indentation depth. The output of the cutting force transducer monitored during the loading procedure is also plotted in the figure. It can be seen that the output of the cutting force

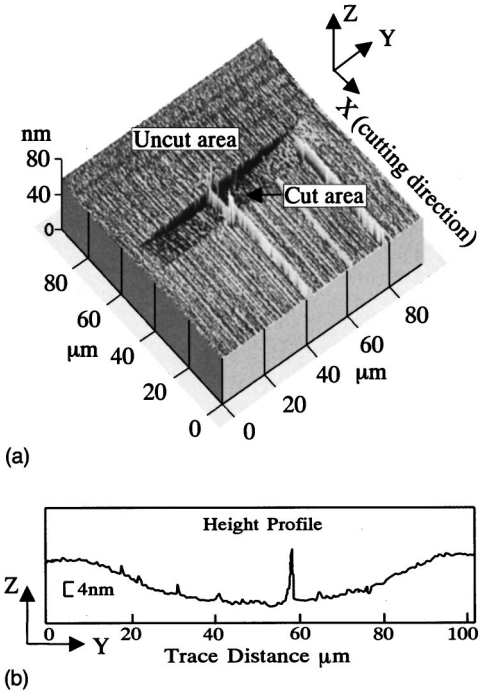

FIG. 11. AFM images of a constant depth of cut. (a) Three-dimensional expression and (b) cross sectional profile of the cut area in the *Y* axis.

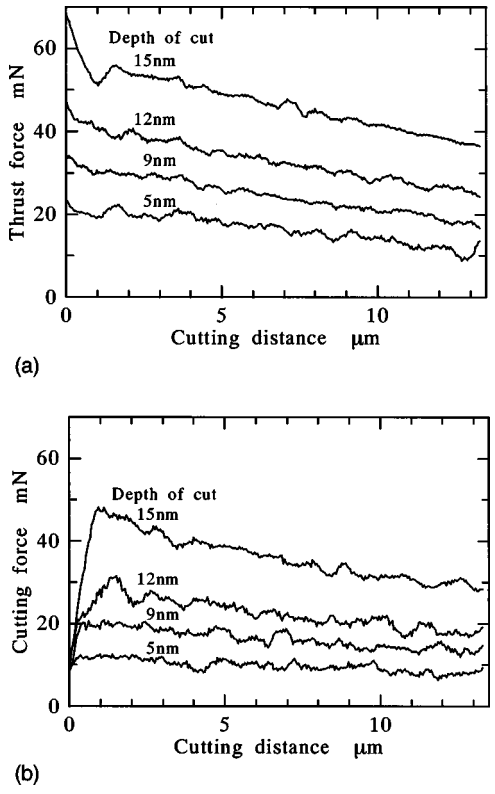

FIG. 12. Output of force transducer during cutting. (a) Output of the thrust force transducer and (b) output of the cutting force transducer.

transducer increased with that of the thrust force. The ratio of the maximum change of the cutting force against that of the thrust force transducer output was used to evaluate the cross sensitivity of force measurement. The cross sensitivity was approximately 3.5%. This value was approximately 2.5 times greater than the design value. The error of the cross sensitivity was caused by errors of manufacturing and assembling the flexures. The infinite frame stiffness of the instrument was another reason for the error of the cross sensitivity.

As described above, the cross-sensitivity measurements were made using a static indent. It should be noted that the situation could be different during a cutting event since the cutting force induces a moment along the axis of flexure 1. It is desired to confirm this by measuring the cross sensitivity using the results of cutting. In this case, careful attention has to be paid to generate a pure cutting force without any thrust force components so that the correct cross sensitivity can be obtained. This will be performed in our future work.

Figure 9 shows the atomic force microscopy (AFM) image of the indent. The sample selected for indentation and cutting experiments was polished (100) single crystal silicon.

Cutting experiments of constant depth of cut were performed. The same cutting tool described above was used. Figure 10 shows the procedure of the cut. At the starting point A, after establishing the tool–sample contact, the sample was moved to the tool in the Z axis until the cutting depth reached the programmed value (step 1). Then the sample was moved along the X axis while keeping the cutting depth constant (step 2). Once the tool reached point B, the sample was moved away from the cutting tool to finish the cut (step 3).

AFM images of a cut are shown in Fig. 11. Figure 11(a) is a three-dimensional expression of the cut, and Fig. 11(b) shows a cross-sectional profile along the Y axis. It can be seen that the cross-sectional profile shown in Fig. 11(b) corresponds to the round nose shape of the tool. The length of cut was approximately 13.5 μm, and the width of cut was about 80 μm. The depth of cut was 15 nm. It should be noted that the width of cut was much wider than the length of cut since the tool was wide (the width of the tool was 2 mm with a 10 mm nose radius). Figure 12 shows the force data with varying depths of cut. Figure 12(a) shows the thrust force data and Fig. 12(b) shows the cutting force data. Only the force data of step 2 in Fig. 10 were shown in the figures. At the starting point, the thrust force showed its largest value, and decreased during cutting. On the other hand, the cutting force increased sharply in the early stage, then decreased during cutting. It can also be seen that the thrust force is greater than the cutting force, which matches the measured results in Ref. 21.

ACKNOWLEDGMENTS

The authors would like to thank John Brien, Jimmie Miller, Stuart Smith, and other members in the Center for Precision Metrology (CPM) for their contributions and discussions. This work was financially supported in part by NSF and the Affiliates of CPM. The support of Osawa Science Foundation to one author (W.G.) is also greatly appreciated.

[1] J. R. Walker, *Machining Fundamentals: From Basic to Advanced Techniques* (Goodheart-Willcox).
[2] E. R. Marshall and M. C. Shaw, Trans. ASME **75**, 51 (1952).
[3] M. Santochi, G. Dini, and M. Beghini, Ann. CIRP **46**, 49 (1997).
[4] Theodore T. Saito, Opt. Eng. **17**, 570 (1978).
[5] B. Krauskoph, Manuf. Eng. 90 (1984).
[6] S. Patterson and E. Magrab, **7**, 123 (1985).
[7] T. A. Dow, M. H. Miller, and P. J. Falter, Precis. Eng. **13**, 243 (1991).
[8] E. Brinksmeier, W. Preub, and O. Riemer, Proceedings of the 3rd International Conference on Ultraprecision in Manufacturing Engineering, Aachen, Germany, 2–6 May 1994, p. 393.
[9] R. Komanduri, N. Chandrasekaran, and L. M. Raff, Ann. CIRP **48**, 67 (1999).
[10] J. A. Patten, K. Flurchick, J. Beeler, and J. Strenkowski, J. Modeling Simul. Mater. Sci. Eng. **2**, 223 (1994).
[11] P. N. Blake and R. O. Scattergood, J. Am. Ceram. Soc. **73**, 949 (1990).
[12] W. S. Blackley and R. O. Scattergood, Precis. Eng. **13**, 95 (1991).
[13] J. C. Morris, D. L. Callathan, J. Kulik, J. A. Patten, and R. O. Scattergood, Am. Ceram. Soc. **78**, 2015 (1995).
[14] K. Nakayama and K. Tamura, J. Eng. Ind. 119 (1968).
[15] W. R. Backer, E. R. Marshall, and M. C. Shaw, Trans. ASME **74**, 61 (1952).
[16] R. J. Hocken, R. Namperumal, P. Pereira, J. Lovingood, R. Edgeworth, A. Sharma, M. Holems, and B. Muralikrishnan, Proceedings of the 1997 ASPE Meeting, Norfolk, VA, 5–10 October 1997, p. 386.
[17] W. Gao, R. J. Hocken, J. A. Patten, J. Lovingood, and D. A. Lucca, Proceedings of the 1999 ASPE Meeting, 31 October–5 November 1999, Monterey, CA, p. 521.
[18] S. Balasubramanium, M.S. thesis, University of North Carolina at Charlotte, Charlotte, NC (1995).
[19] D. A. Lucca, P. Chou, and R. J. Hocken, Ann. CIRP **47**, 475 (1998).
[20] J. A. Bailey and G. Boothroyd, Trans. ASME 54 (1968).
[21] J. D. Drescher and T. A. Dow, Precis. Eng. **12**, 29 (1990).
[22] Model 209A, PCB PIEZOTRONICS Force Transducer Catalog, PCB PIEZOTRONICS, Inc., NY 14043-2495.
[23] J. M. Paros and L. Weisbord, Mach. Des. 151 (1965).